Research Article GU J Sci 37(4): 2025-2034 (2024) DOI: 10.35378/gujs.1313387

Gazi University

Journal of Science

http://dergipark.gov.tr/gujs

Resonant Tunneling Properties in the Sawtooth Triple Barrier Structures

Mehmet BATI[1, *], Gonca CORUH[2]

[1]Recep Tayyip Erdogan University, Department of Physics,53100, Rize, Türkiye
[2]Recep Tayyip Erdogan University, Institute of Graduate Studies, 53100, Rize, Türkiye

Highlights

- The Non-Equilibrium Green Function was used.
- Resonant tunneling event observed.
- Resonance energy levels and transmission probability through the structure were determined.

Article Info

Received: 12 Jun 2023
Accepted: 15 Apr 2024

Keywords

Green Function
Finite difference method
Sawtooth triple barrier
Resonant tunneling
Quantum wells

Abstract

The resonance tunneling properties of sawtooth triple barrier double-well structures were investigated using the non-equilibrium Green's functions method. The dependence of resonance energies on barrier height and width and well widths was investigated. The tunneling feature of the structure under the electric field was investigated. It has been observed that the transmission probability, resonance tunneling energy, and resonance peak intensity are sensitively dependent on the applied electric field and structure parameters. By choosing the appropriate structure, devices that provide resonance transition at the desired energy can be designed in the desired energy level ranges. Thus, this study can provide a basis for switching and oscillator source nano-device designs.

1. INTRODUCTION

With the discovery of the resonant tunneling phenomenon [1], diodes and transistors with low power consumption and high switching speed (on the order of THz) can be produced [2]. There are many theoretical and experimental studies on resonant tunneling devices (RTD), which have many technological applications [3,4]. For the production of structures with resonance tunneling, estimating under which conditions the resonance tunneling event takes place is important in terms of both economy and time. For the investigation of the resonance tunneling properties, the Wigner function method [5], Monte Carlo method [6], the transfer matrix method [7], and the non-equilibrium Green function (NEGF) method [8], quantum simulation techniques are available. NEGF method is one of the most influential and general approaches to describe carrier dynamics in open quantum systems [8].

It is important to note that the performance of resonance tunneling devices (RTD) is extremely sensitive to the atomic scale and related processes at the interfaces that affect the behavior of the material [9-10]. Thanks to the development of nanoscale device manufacturing technology in recent years, high-quality resonant tunneling structures in different geometries (rectangular, parabolic, triangle, etc.) can be produced [11]. Since the rectangular double barrier structure is simple and has been used to test different methods, many studies have been conducted on it [4,12-15]. There are studies examining electron transport in structures with different geometries [14-21]. Electronic transport in the inverse parabolic double barrier structure was studied by Bati using the non-equilibrium Green function method [16]. Ohmukai investigated the dependence of the resonance tunneling properties on the structure parameter in the triangular double barrier structure using the transfer matrix method [17]. In addition, Wang examined this structure under the electric

*Corresponding author, e-mail: mehmet.bati@erdogan.edu.tr

field, again using the transfer matrix method [20], and transmission calculation was made by Luo for this structure [21,22].

The theoretical investigation of tunneling processes in an RTD represents an important source of information for the development of epitaxial crystal growth technology, providing a recipe for the assembly of complex structures such as single and multiple triangular and trapezoidal barriers [23]. These structures allow the use of a triangle barrier optoelectronic switch with resonance tunneling as an important device for optical signal processing [24]. Triangular multi-barrier systems have been used as an alternative candidate for high-speed devices [25-26]. For example, InGaAs/AlAs triple barrier RT heterostructures optimized for operation in the Terahertz frequency range have been investigated [27].

In studies involving three or more barriers, different methods have been studied, and to the best of our knowledge, resonance tunneling in the saw-tooth triple barrier double well (STB) structure has not been investigated. In this study, the resonance tunneling characteristic of the STB structure and its dependence on the electric field bias are examined. The model and method are explained in section 2, numerical results are presented in section 3, and the conclusion is given in section 4.

2. MATERIAL METHOD

The schematic representation of the sawtooth triple barrier potential is shown in Figure 1. V_L V_M, and V_R show left, middle, and right potential barrier height respectively,L_{BL}, L_{BM}, and L_{BR} left, middle, and right potential barrier widths, and L_{WL} and L_{WR} left and right well widths. Each zone boundary location is indicated by L_i (i=1-6).

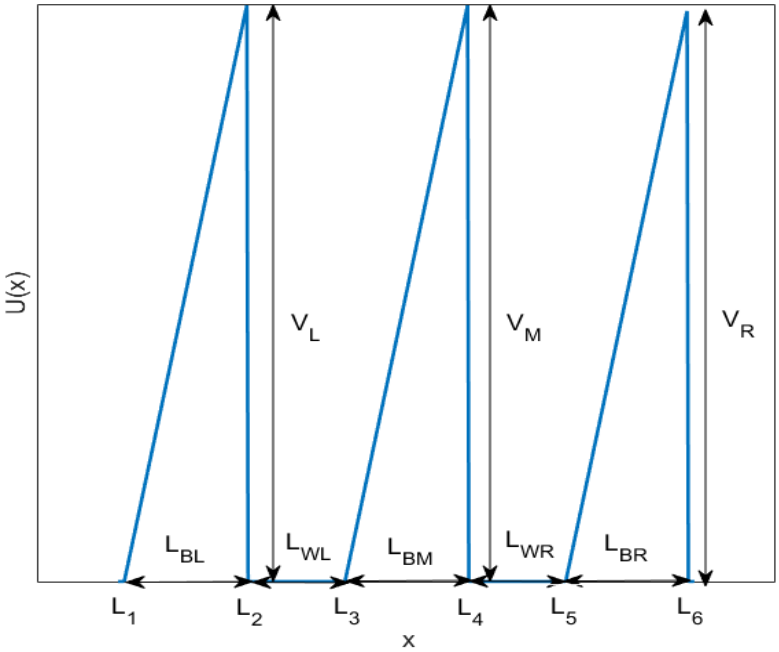

Figure 1. *Sawtooth triple barrier potential structure*

One-dimensional Schrödinger wave equation of the system is

$$-\frac{\hbar^2}{2m^*}\frac{d^2\psi}{dx^2} + U(x)\psi = E\psi. \quad (1)$$

Here, E is the electron energy, m* is the effective mass of the electron, and $\hbar$ is the reduced Planck constant. The functional form of the potential energy profile of the STB structure is given by

$$U(x)=\begin{cases}\left(\frac{V_L}{L_{BL}}\right)(x-L_1), & L_1\le x\le L_2\\ \left(\frac{V_M}{L_{BM}}\right)(x-L_3), & L_3\le x\le L_4\\ \left(\frac{V_R}{L_{BR}}\right)(x-L_5), & L_5\le x\le L_6\\ 0, & otherwise\end{cases} . \tag{2}$$

In our study, we will work with dimensionless parameters to make numerical calculations easier. The lengths will be scaled in terms of the effective Bohr radius ($a_0^*=\frac{4\pi\epsilon_0\hbar^2}{m^*e^2}$), the energies in terms of the effective Hartree Energy ($E_H^*=\frac{\hbar^2}{m^*a_0^{*2}}$). Thus, scaled Schrödinger wave equation is in the dimensionless quantities $\tilde{x}$ and $\widetilde{U}$ takes the form

$$-\frac{1}{2}\frac{d^2\psi}{d\tilde{x}^2}+\widetilde{U}(\tilde{x})\psi=\tilde{E}\psi \ . \tag{3}$$

2.1. Non-Equilibrium Green Function Method

Here, we will briefly summarize the non-equilibrium Green function method to calculate the transition probability. To write the Green function of the system, the space of interest is divided into N parts at $\Delta\tilde{x}$ regular intervals. If the scaled Schrödinger wave equation is written for each point in space using the finite difference method [8, 16] as $\widetilde{U}_n=\widetilde{U}(\tilde{x}_n)$, we find as:

$$-\tilde{t}\psi_{n-1}+\left(2\tilde{t}+\widetilde{U}_n\right)\psi_n-\tilde{t}\psi_{n+1}=E\psi_n. \tag{4}$$

Here $\tilde{t}=\frac{1}{2\Delta\tilde{x}^2}$ is the hopping parameter. If the right and left contact interaction with the device, that is, open boundary conditions, are included in the system, the scaled Schrödinger wave equation becomes the following in matrix form

$$[EI-H-\Sigma_{\mathrm{L}}-\Sigma_{\mathrm{R}}]\{\psi\}=\{S\}\,. \tag{5}$$

$[H]$ and $[I]$ belong to the $(N\times N)$ device region Hamiltonian and identity matrix, respectively and {S}, (N × 1) column matrix. $[\Sigma_{\mathrm{L}}]$ and $[\Sigma_{\mathrm{R}}]$ are self-energy matrices of $(N\times N)$ left and right contacts, respectively. Open form of the Hamiltonian matrix is

$$[H]=\begin{pmatrix}2\tilde{t}+\widetilde{U}_1 & -\tilde{t} & 0 & \cdots & 0 & 0\\ -\tilde{t} & 2\tilde{t}+\widetilde{U}_2 & -\tilde{t} & \cdots & 0 & 0\\ 0 & -\tilde{t} & 2\tilde{t}+\widetilde{U}_3 & \ddots & \vdots & \vdots\\ 0 & 0 & \ddots & \ddots & -\tilde{t} & 0\\ \vdots & \vdots & \ddots & -\tilde{t} & 2\tilde{t}+\widetilde{U}_{N-1} & -\tilde{t}\\ 0 & \cdots & 0 & 0 & -\tilde{t} & 2\tilde{t}+\widetilde{U}_N\end{pmatrix}. \tag{6}$$

Self-energy and source terms are

$$[\Sigma_{\mathrm{L}}]=\begin{pmatrix}-\tilde{t}e^{i\tilde{k}_L\Delta\tilde{x}} & 0 & \cdots & 0\\ 0 & 0 & & 0\\ \vdots & & \ddots & \vdots\\ 0 & & \cdots & 0\end{pmatrix},\ [\Sigma_{\mathrm{R}}]=\begin{pmatrix}0 & \cdots & & 0\\ \vdots & \ddots & & \vdots\\ 0 & \cdots & 0 & 0\\ 0 & & 0 & -\tilde{t}e^{i\tilde{k}_R\Delta\tilde{x}}\end{pmatrix},\ \{\mathrm{S}\}=\begin{pmatrix}-\tilde{t}(e^{i\tilde{k}_L\Delta\tilde{x}}-e^{-i\tilde{k}_L\Delta\tilde{x}}\\ 0\\ \vdots\\ 0\end{pmatrix}.$$

Here $\tilde{k}_L$ and $\tilde{k}_R$ are wave vectors of left and right contact plane waves, respectively. The solution of the Schrödinger wave equation in matrix form in terms of Green's function is $\{\psi\} = [G]\{S\}$. Here the retarted Green's function matrix ([G]) of the system is in closed form expressed as

$$[G] = [(\tilde{E} + i\eta)I - H - \Sigma_{\mathrm{L}} - \Sigma_{\mathrm{R}}]^{-1} . \tag{7}$$

Here η is an infinitesimal positive real number. Transmission coefficient after determining the Green function of the system is calculated as

$$T(\tilde{E}) = Tr[\Gamma_{\mathrm{L}} G \Gamma_{\mathrm{R}} G^{+}] . \tag{8}$$

Here $\Gamma_{\mathrm{L}} = \mathrm{i}[\Sigma_{\mathrm{L}} - \Sigma_{\mathrm{L}}^{+}]$ and $\Gamma_{\mathrm{R}} = \mathrm{i}[\Sigma_{\mathrm{R}} - \Sigma_{\mathrm{R}}^{+}]$ are the broadening matrices.

3. THE RESEARCH FINDINGS AND DISCUSSION

In this work, we assume that our system is constructed with GaAs/AlGaAs materials. The value of effective mass is taken as $0.067m_0$ (where $m_0$is the free-electron rest mass) and relative dielectric constant is taken as 12.7 through the structure [28]. The effective Bohr radius a_0^* and effective Hartree energy E_H^* are computed as 10.1061 nm and 11,2193 meV, respectively. In our work, we use the dimensionless form of energy and length for numerical simplicity. After numeric calculation, we convert units of length and energy into nm and meV, respectively.

Here, the resonance tunneling characteristic of the STB structure will be examined. Figure 2 is plotted for L_{BL}=L_{BM}=L_{BR} *5 nm* and L_{WL} = L_{WR} =*5 nm* without electric field bias (*F = 0*). Figure 2 (a) shows the probability of passing electrons through barriers according to the energy of the incoming electron. When the energy of the electron is smaller than the barrier potential energy, it is observed that all of the electrons coming with the energy close to the energy level in the well can pass. This phenomenon is called resonance tunneling. It is seen that as the barrier heights increase, the number of resonance energy levels in the well increases.

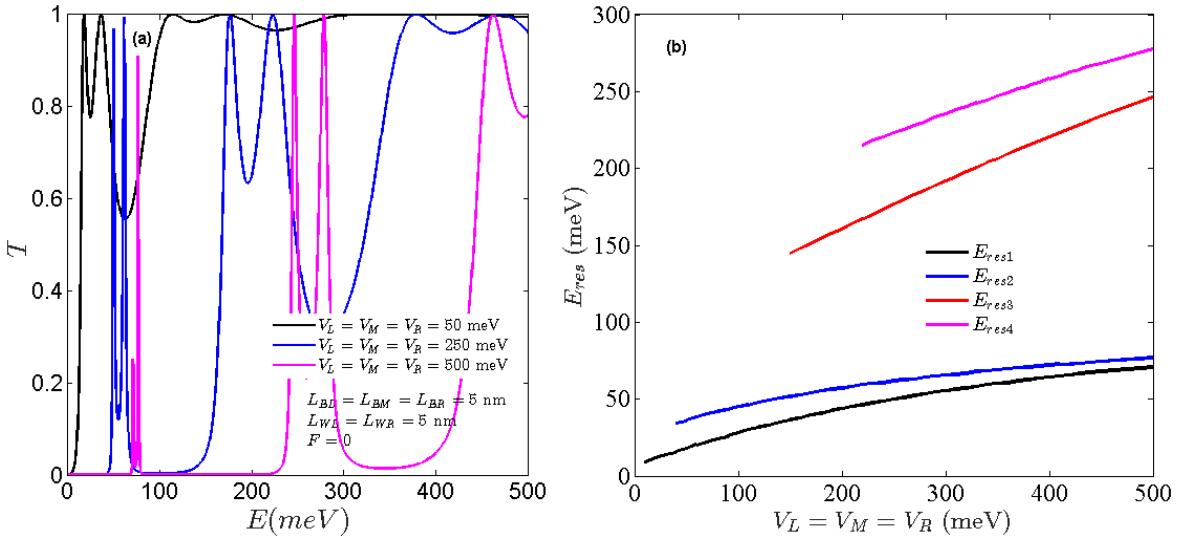

Figure 2. *(color online)* ***a)*** *Graph of the variation of the transmission coefficient with the incident electron energy. Barrier heights vary symmetrically the same V_L= V_M =V_R=50, 250, and 500 meV.* ***b)*** *The graph of resonance energy with barrier heights. System parameters were chosen as L_{BL}=L_{BM}=L_{BR} 5 nm, L_{WL} = L_{WR} =5 nm and F = 0.0*

It is seen that as the barrier heights increase, the number of resonance energy levels in the well increases. Increasing barrier heights increases the blockade in the wells, so resonance peak widths are narrowing. This means that electrons can only pass at certain energies. This is the desired situation in switching devices. In Figure 2 (b), the variation graph of resonance energy levels with barrier heights is plotted. Resonance energy levels shift to higher energies (blue shift) with increasing barrier height.

Figure 3 shows the effect of the middle barrier height on the resonance tunneling event in the STB structure. It is observed that as the height of the middle barriers increases, the resonance energy level shifts towards high energy. It is seen that as the middle barrier height increases, the first and second energy intervals and the 3rd and 4th energy intervals narrow and converge at a certain value. In Figures 2 and 3, it is seen that the probability of transition in resonance energy T (Eres) shows very small changes in the 1st and 2nd resonance energy at the next energy levels close to unity value.

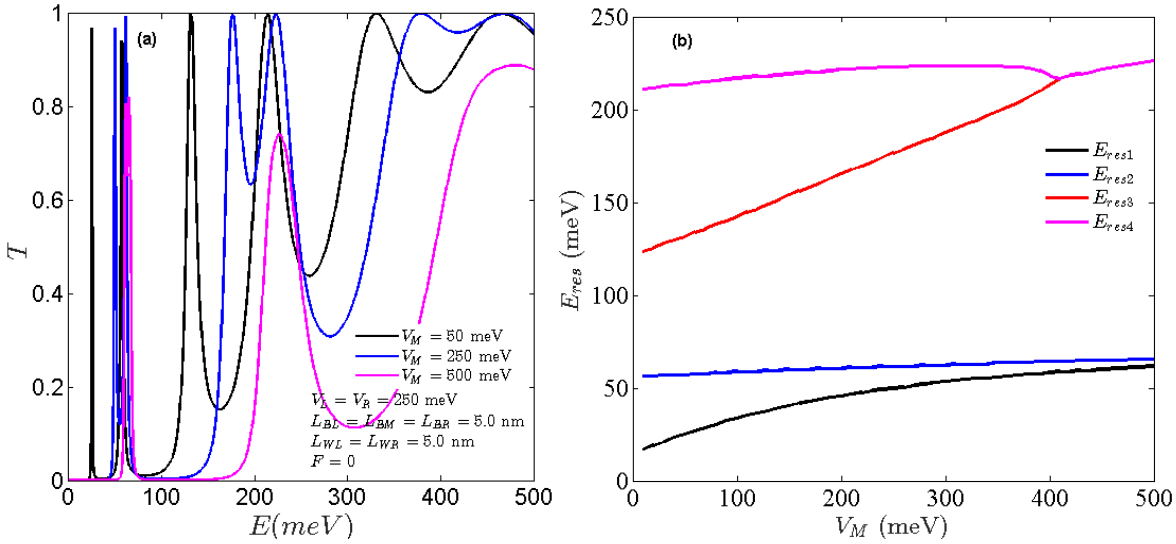

Figure 3. *(color online)* ***a)*** *The variation of the transition probability with respect to the incident electron energy for three different medium potential barrier heights (V_M= = 50, 250, and 500 meV).* ***b)*** *The graph of the resonance energy change depending on the medium potential barrier height. System parameters were chosen as L_{WL}=L_{WR}=5 nm, V_L=V_R=250 meV, and F = 0.0*

In Figure 4 (a), the dependence of the probability of passing electrons on the incident electron's energy for three different barrier thicknesses (L_{BL}=L_{BM}=L_{BR}=*2.0, 5.0,* and *10.0 nm*) are plotted. It is seen that almost all electrons pass through at resonant energy levels (*T (Eres)* ≈*1*). In the case of increased barrier thickness, the resonance peaks are narrowed because the blockade becomes stronger. In Figure 4 (b), the plot of the location of the resonance energy levels depending on the barrier thickness is given. As barrier thickness increases, other energy levels except for the first resonance energy level shift to lower energies (redshift). At the energy level, it increases until the barrier widths match the well widths and then takes a constant value. The difference in energy levels decreases with increasing barrier thickness.

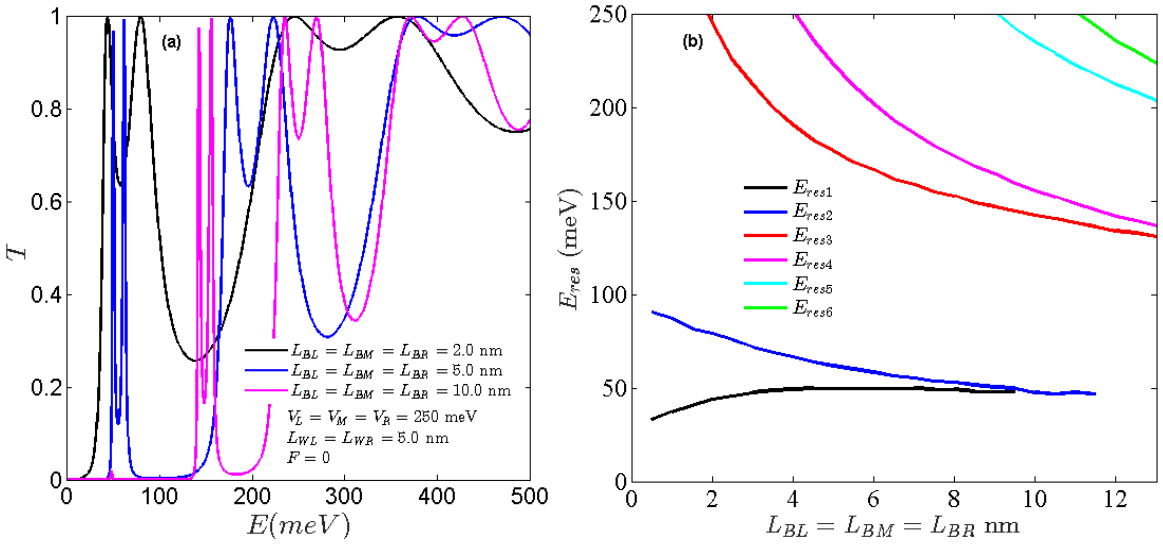

Figure 4. *(color online)* ***a)*** *The variation of the transition probability according to the incident electron energy for three different barrier widths (L_{BL}=L_{BM}=L_{BR}=2.0, 5.0 ve 10.0 nm).* ***b)*** *The graphs of the resonance energy depending on the barrier widths. System parameters were chosen as L_{WL} =L_{WR}=5 nm, V_L=V_M=V_R=250 meV, and F=0.0*

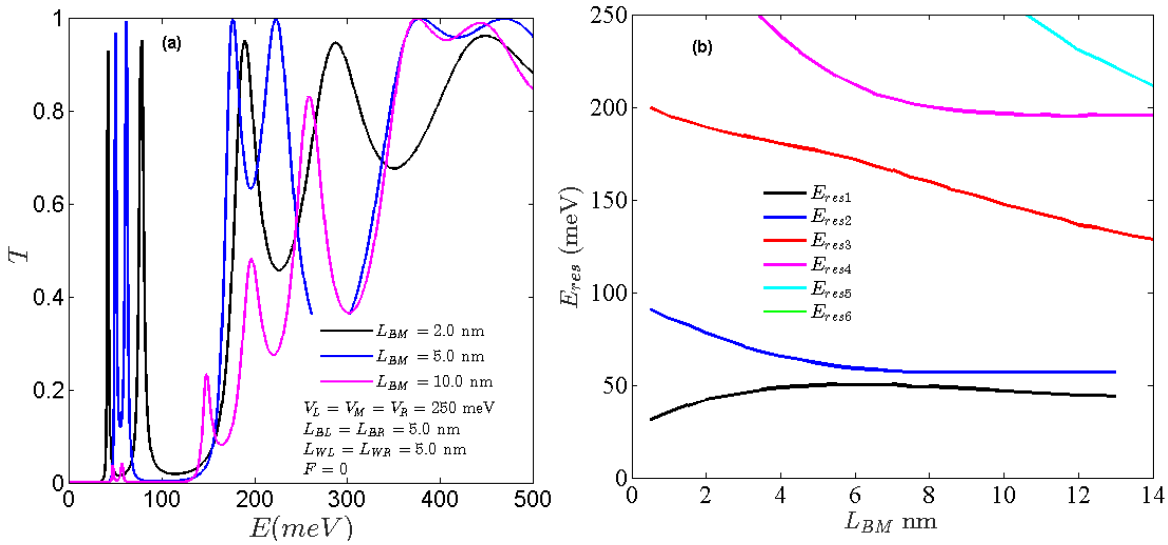

Figure 5. a)*. The variation of the transition probability with respect to the incident electron energy for three medium barrier widths (L_{BM}=2.0, 5.0, and 10.0 nm).* ***b)*** *The graph of change of resonance energy depending on the middle barrier width. The system parameters were chosen as L_{BL} =L_{BR}=5 nm, L_{WL} =L_{WR}=5 nm, V_L=V_M=V_R=250 meV, and F = 0.0*

In Figure 5, when there is no external electric field bias (*F = 0*), system parameters are plotted for L_{BL} =L_{BR}=*5* nm, L_{WL} =L_{WR}=*5 nm*, V_L=V_M=V_R=*250 meV*. In Figure 5 (a), the variation of the transition probability with respect to the incoming electron energy for three medium barrier widths (L_{BM} = *2.0, 5.0,* and *10.0 nm*) is plotted. It is observed that the change in the thickness of the edge barrier *(L_{BL} = L_{BR} = 5 nm)* and the medium barrier thickness increases the asymmetry in the structure and the peak lengths, that is, the probability of passage, are reduced. In Figure 5 (b), the variation of resonance energy levels depending on the middle barrier thickness is plotted. Compared to Figure 4, the change in the middle barrier resulted in the lower energy level of the 3rd energy level and the emergence of the 4th resonance energy level at higher energy.

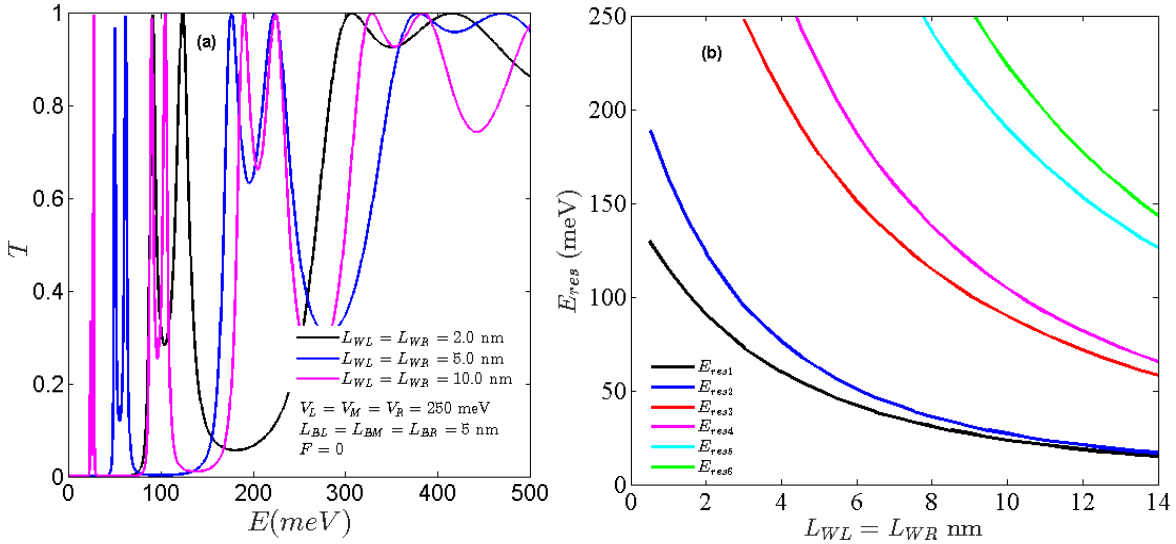

Figure 6. *(color online)* ***a)*** *The variation of the transition probability according to the incident electron energy for three different well widths (L_{WL}= L_{WR}=2.0, 5.0 and 10.0 nm).* ***b)*** *The graph of the resonance energy variation depending on the well widths. System parameters were chosen as L_{BL} = L_{BM} =L_{BR}=5 nm, V_L=V_M=V_R=250 meV, and F = 0.0*

Figure 6 has been drawn to investigate the effect of well widths on resonance tunneling. In Figure 6 (a), the dependence of the probability of passing electrons on the energy of the incident electron for three different well widths (L_{WL}=L_{WR}=*2.0, 5.0,* and *10.0 nm*) is plotted. Figure 6 (b) shows the location of the resonance energy levels depending on the width of the well. As the wells expand, resonance energy levels shift exponentially to lower energy. This happens because the energy levels in the well are formed at lower energies as the well expands. In addition, as the well expands, the number of energy levels remaining in the well increases, so the number of resonance peaks increases due to the resonance energy.

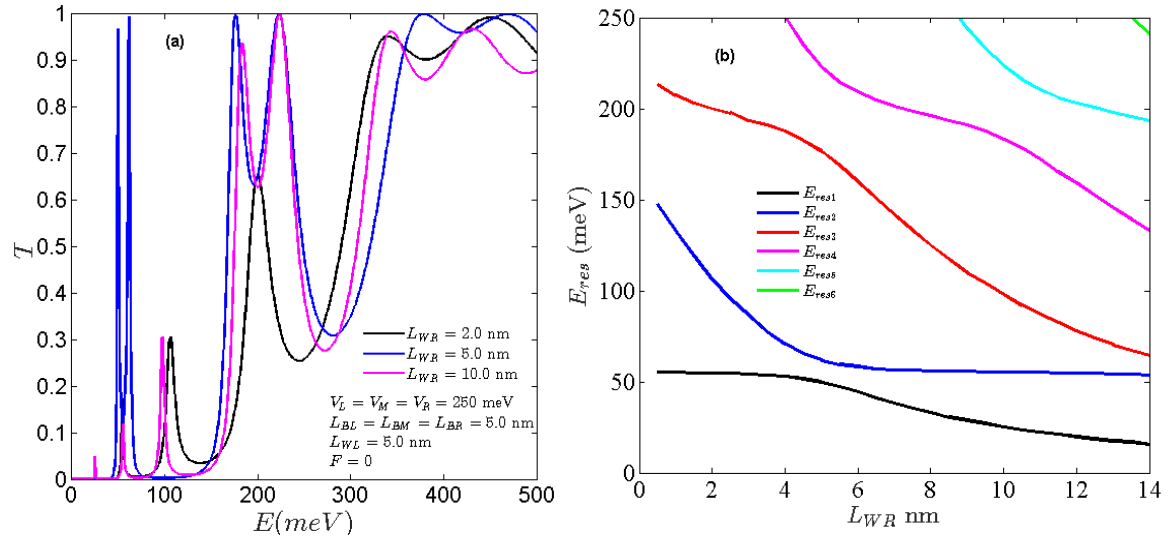

Figure 7. *(color online)* ***a)*** *The variation of the transition probability for three different right well widths (L_{WR}=2.0, 5.0, and 10.0 nm) with respect to the incident electron energy.* ***b)*** *Graph of change of resonance energy depending on the right well width. System parameters were chosen as L_{WR}=5 nm, L_{BL} = L_{BM} =L_{BR}=5 nm, V_L=V_M=V_R=250 meV, and F = 0.0*

Figure 7 is drawn to examine the resonance tunneling event when the width of the right well changes while the left well width is constant (L_{WL}= *5 nm*). In Figure 7 (a), while the well widths are symmetrical at 5 nm, the resonance peak is 1, that is, all incoming electrons can tunnel. In the case of asymmetry between the

widths of the wells, the resonance peak lengths become considerably smaller. In Figure 7 (b), the variation graph of the resonance energy depending on the right well width is plotted. System parameters were chosen as L_{WR}=5 nm, L_{BL} = L_{BM} =L_{BR}=5 nm, V_L=V_M=V_R=250 meV, and F = 0.0. In the case of asymmetry, the exponential change in resonance energies is not observed. However, the increase in the width of the right well also causes resonance energy levels to occur at lower energies. Asymmetry causes a reduction in the length of resonant peaks. This means that the probability of electrons tunneling through specific energy levels decreases.

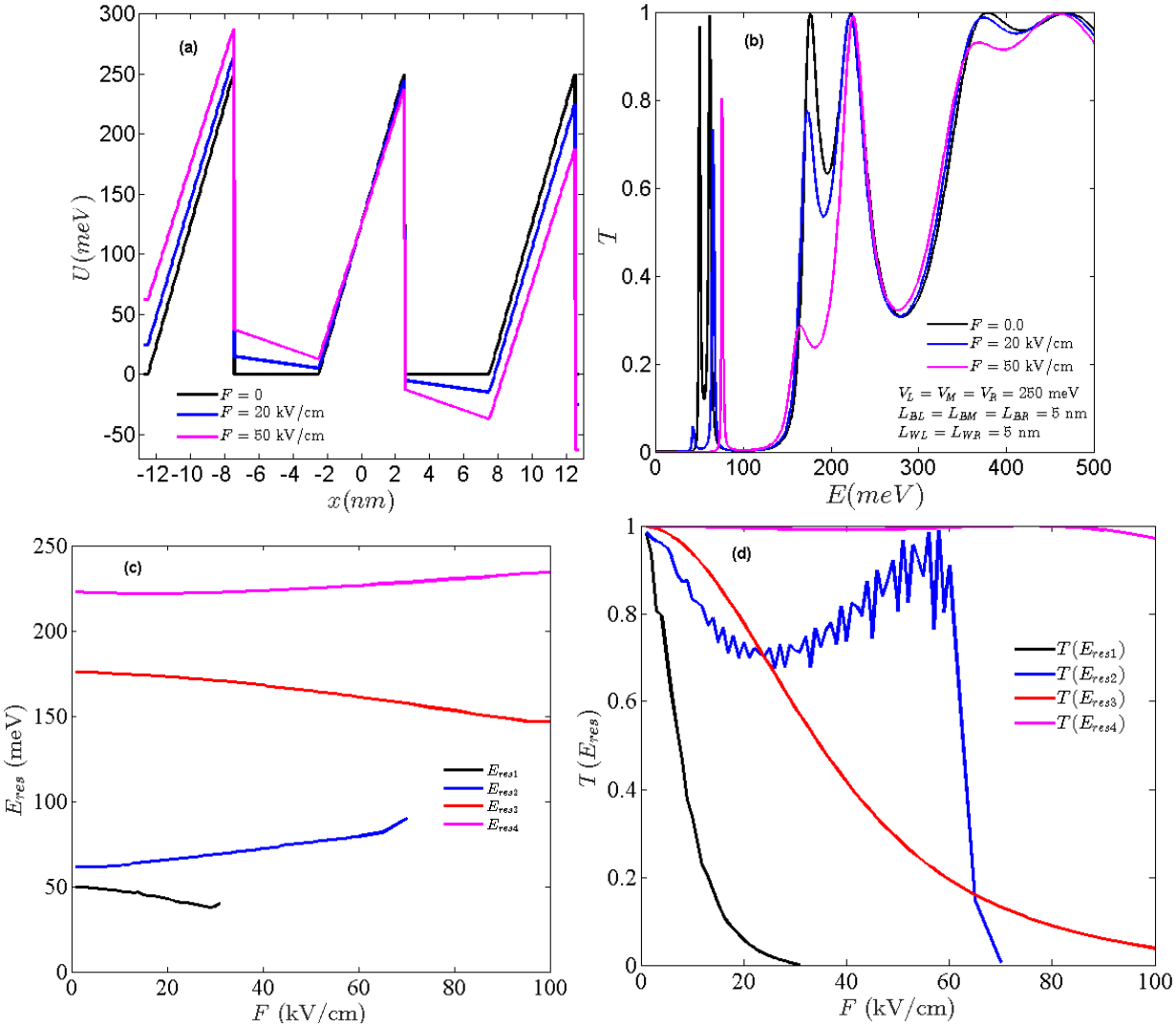

Figure 8. *(color online)* ***a)*** *TBS under the electric field bias resonance energy levels* ***b)*** *The variation of the transition probability for three different electric field bias (F=0.0, 20, and 50 kV/cm^2) with respect to the incident electron energy.* ***c)*** *Graph of change of resonance energy depending on electric field bias* ***d)*** *Change of resonance peak amplitude with electric field. System parameters were selected as L_{WL}= L_{WR}=5 nm L_{BL}=L_{BM} =L_{BR}=5 nm and V_L=V_M=V_R=250 meV*

Figure 8 (a) shows the potential shape in case of application of electric field bias (eFx) when F = 0, 20, and 50 kV / cm. System parameters were chosen as L_{WL}= L_{WR}=5 nm, L_{BL}=L_{BM} =L_{BR}=5 nm, and V_L=V_M=V_R=250 meV. Figure 8 (b) shows the variation of the resonance peak amplitude with the electric field bias. It is seen that as the electric field bias increases, the resonance peak amplitude decreases. Figure 8 (c) shows the changes in resonance energy levels due to electric field bias. It is observed that as the electric field bias increases, the 1st and 3rd resonance energy levels, that is, the right well energy levels, shift to lower energy. Energy levels 2 and 4 are shifting to higher energy. In Figure 4 (d), the variation of the probability of transition in the resonance energy level due to electrical bias is plotted. The graph shows

that the 1st and 3rd resonance peak amplitudes disappear as the electric field bias increases. It is seen that the transition from resonant energy is fluct uating and the transition stops in high electric field bias. In the resonance energy peak, there is a complete transition. The RT effect can be made switching in nano-devices. The transmission can be controlled by increasing or decreasing the particle energy, thanks to particles with certain energies passing.

4. RESULTS

The dependence of the resonance energy on the well width, barrier widths, and heights in the saw tooth double barrier structure was analyzed using the finite difference method based on non-equilibrium Green's function method. While the electric field bias is very weak, all particles in the resonance tunneling energy are tunnels, in other words, the transmission coefficient is one. When the symmetry is broken or when the electric field intensity is increased in a symmetrical structure, the possibility of transmission decreases, i.e. the resonance tunneling peak intensity decreases. While resonant tunneling energy shifts to lower energy values as the well width increases, it shifts to higher energies with the increase of barrier heights. Changes in barrier heights have little or no effect on resonance peak intensity. As a result, useful device applications can be developed by controlling the resonance tunneling characteristic with these parameters in triple barrier structures.

CONFLICTS OF INTEREST

No conflict of interest was declared by the authors.

REFERENCES

[1] Esaki, L., “New Phenomenon in Narrow Germanium p-n Junctions”, Physical Review, 109: 603-604, (1958).

[2] Ferry, D.K., Goodnick, S. M., Bird, J., “Transport in nanostructures”, Cambridge University Press, Cambridge, (2009).

[3] Regan, B.C., Aloni, S., Jensen, K., Zettl, A., “Surface-tension-driven nanoelectromechanical relaxation oscillator”, Applied Physics Letters, 86: 123119, (2005).

[4] Levi, A.F.J., “Applied Quantum Mechanics”, Cambridge University Press, Cambridge, (2012).

[5] Wigner, E., “On the quantum correction for thermodynamic equilibrium”, Physical Review, 40: 749-759, (1932).

[6] Shifren, L., Ferry, D., “Particle Monte Carlo simulation of Wigner function tunneling”, Physics Letters A, 285(3): 217-221 (2001).

[7] Tsu, R., Esaki, L., “Tunneling in a finite superlattice”, Applied Physics Letters, 22(11): 562-564, (1973).

[8] Datta, S., “Quantum transport: atom to transistor”, Cambridge University Press, Cambridge, (2005).

[9] Shahjahan, M., Khatun, M.H., Sawada, K., Ishida, M., “TEM study of RTD structure fabricated with epi-Si/gamma-Al2O3 heterostructure”, Thin Solid Films, 518: 2295-2298, (2010).

[10] Kitabaysahi, H., Waho, T., Yamamoto, M., “Resonant interband tunneling current in InAs/AlSb/GaSb/AlSb/InAs diodes with extremely thin AlSb barrier layers”, Applied Physics Letters, 71: 512, (1997).

[11] Harrison, P., "Quantum wells, wires and dots: theoretical and computational physics of semiconductor nanostructures", John Wiley & Sons, New York, (2010).

[12] Miyamoto, K., Yamamoto, H., "Resonant tunneling in asymmetrical doublebarrier structures under an applied electric field", Journal of Applied Physics, 84(1): 311-318, (1998).

[13] Abdalla, A.S., Eisa, M.H., Alhathlool, R., Aldaghri, O., "Quantum resonant tunneling in semiconductor double-barrier structure", Optik, 170: 314-320, (2018).

[14] Encomendero, J., Protasenko, V., Sensale-Rodriguez, B., Fay, P., Rana, F., Jena, D., Xing, H.G., "Broken Symmetry Effects due to Polarization on Resonant Tunneling Transport in Double-Barrier Nitride Heterostructures", Physical Review Applied, 11: 034032, (2019).

[15] Almansour, S., "Theoretical study of electronic properties of resonant tunneling diodes based on double and triple AlGaAs barriers", Results in Physics, 17: 103089, (2020).

[16] Bati, M., Sakiroglu, S., Sokmen, I., "Electron transport in electrically biased inverse parabolic double-barrier structure", Chinise Physics B, 25(5): 057307, (2016).

[17] Ohmukai, M., "Triangular double barrier resonant tunneling", Materials Science and Engineering: B, 116: 87-90, (2005).

[18] Bati, M., "Electronic Transport and Resonant Tunneling Properties of Hyperbolic Poschl-Teller Double-Barrier Structures", Journal of Computational and Theoretical Transport, 48: 66-76, (2019).

[19] Bati, M., "Resonant tunneling properties of inverted Morse double quantum barrier", Chinese Journal of Physics, 56: 593-597, (2018).

[20] Wang, H., Xu, H., Zhang, Y., "A theoretical study of resonant tunneling characteristics in triangular double-barrier diodes", Physics Letters A, 355(6): 481-488, (2006).

[21] Luo, M., Yu, G., Xia, L., "Calculation of conductance for triangular multi-barrier structure in a constant electric field", Superlattices and Microstructures, 83: 168-175, (2015).

[22] Luo, M., Yu, G., Lin, Y., Su, J., "Calculation of current density for triangular multi-barrier structure in a constant electric field", Superlattices and Microstructures, 74: 78-84, (2014).

[23] Wang, H.M., Xu, H.Z., Zhang, Y.F., "A theoretical study of resonant tunneling characteristics in triangular double-barrier diodes", Physics Letter A, 355: 481-488, (2006).

[24] Sakata, H., Utaka, K., Matsushima, Y., "Novel bistable device Resonant-tunneling triangular-barrier optoelectronic switch (R-tops)", Electronics Letters, 30: 1714-1716, (1994).

[25] Guo, D.F., "Negative-differential-resistance characteristics in a triangularbarrier resonant tunnelling switch", Semiconductor Science and Technology, 13: 231-235, (1998).

[26] Leite, T.N., and de Oliveira, H.P., "Tunneling Processes in a Triangular Multibarrier Semiconductor Heterostructure", IEEE Transactions on Electron Devices, 58: 716-719, (2011).

[27] Allford, C.P., and Buckle, P.D., "Strain Compensated InGaAs/AlAs Triple Barrier Resonant Tunneling Structures for THz Applications", IEEE Transactions on Terahertz Science and Technology, 7: 772-779, (2017).

[28] Sze, S.M. "Physics of Semiconductor Devices", Wiley, New York, (1981).